Arabian Journal of Chemistry (2022) **15**, 104207

King Saud University

Arabian Journal of Chemistry

www.ksu.edu.sa
www.sciencedirect.com

ORIGINAL ARTICLE

Electrospun nickel nanoparticles@poly(vinylidene fluoride-hexafluoropropylene) nanofibers as effective and reusable catalyst for H_2 generation from sodium borohydride

Abdullah M. Al-Enizi [a], M.M. El-Halwany [d,*], Shoyebmohamad F. Shaikh [a], Bidhan Pandit [c], Ayman Yousef [b]

[a] *Department of Chemistry, College of Science, King Saud University, Riyadh 11451, Saudi Arabia*
[b] *Department of Mathematics and Physics Engineering, Faculty of Engineering at Mataria, Helwan University, Cairo 11718, Egypt*
[c] *Department of Materials Science and Engineering and Chemical Engineering, Universidad Carlos III de Madrid, Avenida de la Universidad 30, 28911 Leganés, Madrid, Spain*
[d] *Department of Mathematics and Physics Engineering, Faculty of Engineering, Mansoura University, El-Mansoura, Egypt*

Received 13 May 2022; accepted 14 August 2022
Available online 23 August 2022

KEYWORDS

Ni@PVDF-HFP;
Nanofibers;
Electrospinning;
Sodium Borohydride;
Hydrogen

Abstract Nickel nanoparticles (Ni NPs) supported on Poly(vinylidene fluoride-*co*-hexafluoropropylene) nanofibers (PVDF-HFP NFs) were successfully synthesized through electrospinning and in-situ reduction of Ni^{2+} salts into the surface of PVDF-HFP NFs to form metallic Ni NPs@PVDF-HFP NFs. Different percentages of nickel acetate tetrahydrate (NiAc) (10 %, 20 %, 30 %, 40 % wt.) based PVDF-HFP. The formation of tiny metallic Ni NPs @PVDF-HFP membrane NFs was demonstrated using standard physiochemical techniques. Nanofibers membranes have demonstrated good catalytic activity in H_2 production from sodium borohydride ($NaBH_4$). The sample composed of 40 %wt Ni showed the highest catalytic activity compared to the other formulations. Whereas 103 mL of H_2, from the hydrolysis of 1.34 mmol $NaBH_4$, was produced using 40 wt% NiAc compared to 68 mL, 81 mL, and 93 mL for 10 wt%, 20 wt%, and 30 wt% NiAc, respectively, in 60 min at 25 °C. The hydrogen generation has been enhanced with an increase in the Nanofibers membrane amount and reaction temperature. The latter results in a low activation energy (23.52 kJ mol^{-1}). The kinetics study revealed that the reaction was pseudo-first-order in sodium borohydride concentration and catalyst amount. Furthermore, the catalyst exhibits

* Corresponding author.
E-mail address: aymanyousef84@gmail.com (A. Yousef).
Peer review under responsibility of King Saud University.

Production and hosting by Elsevier

https://doi.org/10.1016/j.arabjc.2022.104207

satisfactory stability in the hydrolysis process for ten cycles. Because of its easy recyclability, the introduced catalyst has a wide range of potential applications in the generation of H_2 from sodium borohydride hydrolysis.

1. Introduction

The development of sustainable, clean, and environmentally friendly energy is becoming increasingly important to address the growing threat of energy exhaustion and greenhouse gas emissions **that contribute to dangerous climate change** (Kılınç and Sahin, 2018; Chen et al., 2011). Hydrogen (H_2) is a potential alternative to meeting the world's increasing energy demand while also serving as an eco-friendly energy carrier molecule for future applications (Kılınç and Sahin, 2018). From the standpoint of the application, the safe generation, storage, and transportation of H_2 are necessary conditions (Cai et al., 2016). Chemical hydrides are considered suitable materials for all of the applications as mentioned above. Chemical hydride hydrolysis is gaining popularity as a potential in-situ H_2 supply method for proton exchange membrane fuel cells (PEMFCs) (Crisafulli et al., 2011; Kassem et al., 2019). Amongst chemical hydrides, sodium borohydride ($NaBH_4$) is a preferable material for H_2 storage and generation due to its high H_2 capacity (~10.9 wt%) (Lee et al., 2021; Abdelhamid, 2021; Abdelhamid, 2021), high stability in alkaline solution (Ritter, 2003), pure H_2 production (Kim, 2004), recycling of the by-products (Calabretta and Davis, 2007; Santos, 2010; Santos and Sequeira, 2011) and non-flammable and less expensive (Chinnappan et al., 2011). Theoretically, one mole of $NaBH_4$ can produce four moles of H_2 in water (Eq. (1)) (Yao et al., 2020):

$$NaBH_4 + 2H_2O \rightarrow catalyst\, 4H_2 + NaBO_2 \quad (1)$$

Self-hydrolysis of $NaBH_4$ is slow; thus, the addition of an appropriate catalyst can greatly accelerate the hydrolysis reaction (Wechsler et al., 2008). Hitherto, various nano-catalytic materials (e.g., Pt, Ru, Rh, Pd, Ni, Co, Fe, and their alloys) have been used in the hydrolysis reaction of $NaBH_4$ (Dinc et al., 2012; Oh et al., 2015; Shen et al., 2015; Ding et al., 2010; Park et al., 2008; Arzac et al., 2012; Lee et al., 2021; Larichev et al., 2010; Xu et al., 2008; Chen and Kim, 2008). Ni-based catalysts provide objective interest as a catalyst because of their low cost and environmentally friendly construction (Ozay et al., 2011). However, because Ni has a high energy surface and magnetic properties, it must be dispersed and stabilized by appropriate materials to achieve long-term durability without the formation of aggregates (Wang et al., 2021). **Furthermore, the formation of $NaBO_2$ as a by-product during $NaBH_4$ hydrolysis leads to deactivation of the catalyst surface** (Chinnappan et al., 2011). Because metal-based catalysts are typically used in powder form, they are inconvenient for start-and-stop applications. Separation of the catalyst powder from the reaction media and the possibility of catalyst particle aggregation significant practical issues (Chinnappan and Kim HJIjohe, 2012). The supporting materials significantly impact catalyst activity and durability (Li et al., 2012). Polymer substrates, as we know, have flexible design structures and are easily separated from reactants. As a result, various Ni–polymer hybrids with varying morphologies have been synthesized using various preparation methods (Kılınç and Sahin, 2018; Chen et al., 2011; Cai et al., 2016; Sagbas, 2012; Seven and Sahiner, 2014; Liu et al., 2013; Yan et al., 2009; Chen et al., 2015; Cai et al., 2016; Özhava et al., 2015; Chen et al., 2009). They demonstrated a high value in H_2 generation from NaBH4 while overcoming the mentioned above. As we know, the method of preparation and the morphology of the catalysts directly impact their catalytic activity. Polymer nanofiber membrane (PNFM) have been proposed as supporting materials for various NPs in various chemical reactions. When compared to other supporting materials, PNFM are easily recyclable and reused with high efficiency. Nanofibers are able to form a highly porous mesh therefore their usage is almost endless (Chinnappan et al., 2011). Li et al (Li et al., 2014), They prepared composite nanofibers by immobilizing Cobalt (II) chloride on polyacrylonitrile NFs, which demonstrated excellent catalytic performance and stability in H_2 generation from NABH4 solutions. Kim and his group developed hybrid NFs based on polyvinylidene fluoride (PVDF) as a support substrate in the production of H_2 from $NaBH_4$ (Chinnappan et al., 2011); Y-zeolite/$CoCl_2$-PVDF (Li et al., 2012), dicationic tetrachloronickelate (II) anion (dicationic ionic salt [C6(mpy)2][NiCl4]$_2$)-PVDF (Chinnappan and Kim HJIjohe, 2012); Ni NPs-PVDF (Sheikh et al., 2011). They found that the prepared hybrid membranes have good catalytic activity and are reusable. Electrospun poly(vinylidene fluoride-*co*-hexafluoropropylene) (PVDF-HFP) has recently been introduced as a polymer electrolyte and membrane in various applications (e.g., fuel cells, dye-sensitized solar cells, lithium-ion batteries, and water separation) (Raghavan et al., 2008; Mališ et al., 2013; Vijayakumar et al., 2015; Zhang et al., 2021; Tian and Jiang, 2008). In comparison to other host polymers (e.g. poly(ethylene oxide) (PEO), poly(ethylene glycol), poly(urethane acrylate), (PVdF), poly(methyl methacrylate), and PEO-modified poly(methacrylate)), PVDF-HFP is regarded as the most suitable host polymer for preparing hybrid composites (Raghavan et al., 2008). It has a high affinity to absorb electrolyte solution with good chemical and electrochemical stability (Zhang et al., 2014). In this study, we exploited the hydrophobic properties of PVDF-HFP to deposit NPs on its surface because the salt contains tetrahydrate, which makes deposition of NPs on the surface preferable to embedding NPs supporting on PVDF-HFP NFs. This hypothesis has two consequences: (1) reduce polymer crystallinity and (2) increase solution uptake, which may improve contact between the $NaBH_4$ and catalyst surface (Raghavan et al., 2008). Accordingly, PVDF-HFP is considered an efficient supporting material for NPs which is a chemically stable and easily recyclable polymer. To our knowledge, no research has been conducted on the preparation of Ni NPs@PVDF-HFP membrane NFs for H_2 production from $NaBH_4$ hydrolysis as an efficient and easily reusable catalyst material. Metallic Ni nanoparticles embedded in PVDF-HFP NFs were investigated as non-precious catalysts for H_2 generation from $NaBH_4$ in this study. The NFs presented here were prepared using an electrospinning technique and a chemical reduction process. Typically, electrospun nanofibers composed of NiAc and PVDF-HFP were dried and then reduced in-situ with $NaBH_4$ to form Ni NPs supporting on PVDF-HFP NFs. The in-situ reduction process has been done in methanol solution. The utilized physicochemical characterizations indicated that the reduction process leads to form Ni supporting on the PVDF-HFP NFs.

2. Experimental details

2.1. Materials

Nickel (II) acetate tetrahydrate (NiAc, 98 % assay), poly (vinylidene fluoride-*co*-hexafluoropropylene) ((PVDF-HFP), 98 % assay) with a molecular weight of 65,000 g/mol, and sodium borohydride ($NaBH_4$, 98 % assay) were purchased from Aldrich Co., USA. N, *N*-dimethylformamide (DMF, reagent grade, 99 % assay), and acetone were brought from

Fluka. All these chemicals were used without further purification.

2.2. Preparation of NiAc@PVDF-HFP MNFs

First, 15 wt% PVDF-HFP solutions were prepared by dissolved 1.5 gm PVDF-HFP in a mixture of DMF and acetone (4:1 wt ratio). Four different percentages of NiAc-based PVDF-HFP (10 % (HFB-10), 20 % (HFB-20), 30 % (HFB-30), and 40 % wt. (HFB-40)), NiAc was dissolved in a determined amount of DMF before added to the PVDF-HFP solution, have been added to PVDF-HFP solution in the separated laboratory glass bottles. The solutions were kept in the magnetic stirrer overnight. The prepared sol-gels were subjected to the lab-scale electro-spinner machine. The sol–gel was placed in a plastic capillary syringe. A copper wire was inserted inside the syringe from one side, and the other side was connected to a high-voltage power supply (positive electrode). The negative electrode was connected with a ground iron drum covered by aluminum foil to collect electrospun NF mats. 20 kV voltage was applied between syringe and drum. The collected electrospun NF mats were dried at 30 °C under a vacuum overnight. The pristine PVDF-HFP-free NiAc membrane has been prepared with the same procedure.

2.3. *Chemical reduction of NiAc supporting PVDF-HFP NFs*

Typically, determining amounts from prepared electrospun NF mats were immersed in a 500 mL beaker containing methanol solution. A determined amount of $NaBH_4$ was added to the previous solution. The molar ratios between metals precursor and $NaBH_4$ were adjusted at 1:5 to obtain a full reduction reaction. As soon as the mat was attached to the $NaBH_4$ solution, the color was changed from green to black, and the membranes looked like a black dying piece of cloth (Fig. 1). The mat was left in solution until the gas bubble stopped. The produced mat was washed three times with **deionized** water and ethanol to remove any residues. Finally, the reduced mat was dried under vacuum at 30 °C overnight.

2.4. Characterization

The morphology of the prepared catalytic NFs was observed by scanning electron microscope (SEM, Hitachi S-7400, Japan), equipped with energy dispersive X-ray (EDX) **before inspection samples were coated with gold**. For the investigation of the morphology of PVDF-HFP membrane NFs and their interactions with the Ni NPs, Fourier transform infrared (FTIR), using the smart ATR-FTIR model "Nicolet iS 10" (Thermo Fisher Scientific, MA USA) equipped with the specular reflectance. The scanning range was 400–3500 $cm^{-1,}$ and the samples were placed on the top of the spectrophotometer. The catalysts' crystalline structure and crystal size were determined by X-ray diffraction (Rigaku Co., Japan) with Cu Kα (λ = 1.54056 Å). An X-ray photoelectron spectroscopy analysis (XPS, AXIS-NOVA, Kratos Analytical, UK) was conducted with the following conditions: base pressure of 6.5×10^{-9} Torr, resolution (pass energy) of 20 eV, and scan step of 0.05 eV/step. A thermogravimetric analyzer (TGA) was used for the thermal analysis and stability of NFs samples with a heating rate of 10 °C/min and nitrogen flow rate of 20 mL/min. The temperature range for the analysis was set between room temperature and 900 °C.

2.5. Catalytic hydrolysis of NaHB4 using prepared nanofibers

The H_2 gas produced during the reaction was passed through a tube and collected in an inverted burette using the water displacement method. The volume of hydrogen generated was calculated by measuring the change in the height of the water level in the burettes at different time intervals. The catalytic reaction was carried out in a reactor made up of Pyrex round bottom flask reactors. The volume of H_2 produced was calculated using the water displacement method. The reaction vessel was immersed in a temperature-controlled water bath to control reaction temperature. The determined concentration of aqueous $NaBH_4$ solution and amount of catalyst was added to the reaction vessel. The hydrolysis reaction's kinetics investigated by varying the amount of catalyst, $NaBH_4$ amount, and temperature. It also investigated the long-term durability of the introduced membrane NFs via the recycling process.

3. Results and discussion

Proposing the electrospinning technique for preparing polymeric nanofibrous membranes could display many distinct features, including increased interconnectivity, flexibility, excellent porosity, and extraordinary surface-to-volume ratios (Gibson et al., 2001; Yousef et al., 2012). Among the commonly used polymeric chemicals for fabricating these films, PVdF-HFP is the most preferred due to its semi-crystalline nature, good thermal stability, increased dielectric constant, and hydrophobicity besides its piezo and pyroelectric characteristics (Shin et al., 2010; Kumar GGJJoMC. , 2011). Fig. 2 **a and b** show the low and high magnifications SEM image of electrospun PVdF-HFP NF mats after drying; as shown in the figure, a good nanofibrous structure without any beads are formed. Furthermore, nano-cracks appeared on the surface of the NFs. This could be due to the rapid evaporation rate of the acetone solvent during the electrospinning process before NFs reach the drum's surface that helps produce this nano-cracks structure as a suitable site for the nucleation of Ni crystals. The water content of the used nickel precursor salt appreciably improved the hydrophilicity of fabricated polymeric membranes with enhanced demixing rate inside the liquid–liquid phases to favor the formation of numerous pores onto their structure (Chen et al., 2015). Afterward, the analyte molecules could be easily trapped in these pores with the lowest diffusion resistance and facilitate the H_2 evolution.

Moreover, the presence of metals salts has a beneficial role in increasing the electrical conductivity and the gelation of the polymer solution with the generation of maximum elongation of a jet along its axis to produce extremely small-sized polymeric nanofibers (Kang et al., 2014) finally. During the in-situ reduction of Ni(II) ions used $NaBH_4$ as a powerful and effective reducing agent in methanol media, metallic Ni NPs are produced and deposited onto the PVdF-HFP membrane surface. SEM images of electrospun Ni@PVdF-HFP NF membranes NFs were shown in **Fig. [2c (HFB-10), d (HF-B20), e (HF-B30), and f (HF-B40)]**, the inset show the high magnifications SEM images. As shown in the figure, the rough

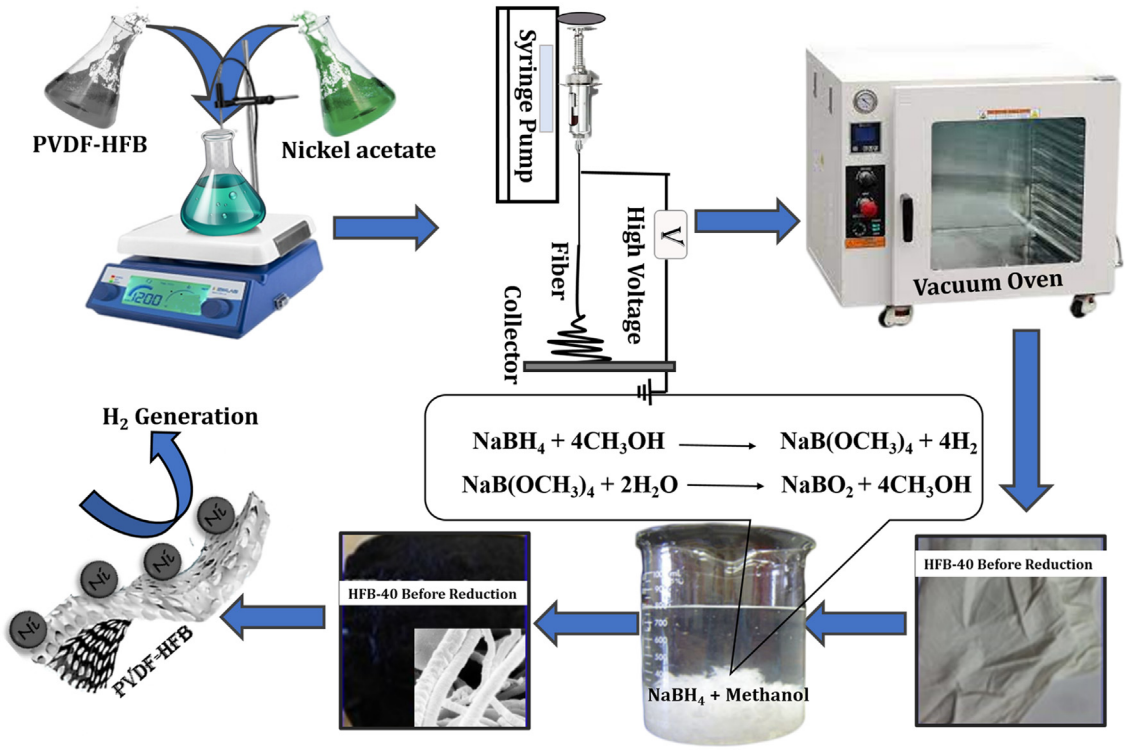

Fig. 1 Scheme showing the preparation of Ni-PVDF-HFP and H_2 generation from $NaBH_4$.

and beads-free NFs are formed. Furthermore, reduced Ni ions are covered the surface of PVdF-HFP NF mats as they built up based on the nano-cracks present on PVdF-HFP NFs surface.

During the methanolysis process (Aydın et al., 2020), sodium tetra methoxy borate ($NaB(OCH_3)_4$) is formed as a by-product (**Equation (2)**). During washing, sodium tetra methoxy borate reacts with water (**Equation (2)**) to produce sodium borate and methanol that wash out with excess water.

$$NaBH_4 + 4CH_3OH \rightarrow NaB(OCH_3)_4 + 4H_2 \quad (2)$$

$$NaB(OCH_3)_4 + 2H_2O \rightarrow NaBO_2 + 4CH_3OH \quad (3)$$

Using methanol for dehydrogenating $NaBH_4$ has advantages over the use of water. One of them is related to the nature of the by-product. In methanolysis, $NaB(OCH_3)_4$ forms. Unlike $NaB(OH)_4$, $NaB(OCH_3)_4$ does not have the propensity to polymerize into polyborates. **Avoiding the $NaB(OH)_4$ precipitation inhibits catalyst poisoning** (Aydın et al., 2020; Lo et al., 2007). Hongming et al. (Zhang, 2020), prepared ultrafine Co NPs @ carbon nanospheres using hydrothermal and reduction processes as an efficient catalyst for H_2 production from $NaBH_4$ hydrolysis. They indicated that the reduction of Co ions in the ethanol solution media is better than in water media, in which partial $NaBO_2$ was precipitated out with the Co NPs due to the insolubility of NaBO2 in ethanol could separate and further prevent the agglomeration of the Co nanoparticles. At last, the $NaBO_2$ was washed off with DI water. The electrospun Ni^{2+}/PVdF-HFP membranes had white-colored surfaces. The chemical reduction of these metallic ions tends to change the color of their related polymeric membranes into a black-look-like black dying piece of cloth (Fig. 1), which suggests the growth of tiny Ni NPs on the surface of PVdF-HFP membranes. In other words, the complete coverage of PVdF-HFP membranes surface with skin layers of black nickel dots might resemble the shell "Ni nanoparticles"-core "polymeric film" arrangements. An elemental mapping image of the HFP-40 membrane was presented in Fig. (3 a, b, and c). It is clear that the high distribution of Ni NPs around the membrane NFs, is confirmed by the SEM images. EDX chart of HFP-40 membrane was presented in Fig. (4 a and b). The related peaks of carbon, nickel, and fluorine were detected to ensure the successful fabrication of these composite membranes. The XRD study in Figs explored the crystal structure of PVdF-HFP and HFP-40 membrane**s. (5 a and b)**, respectively. Three main diffraction planes were observed at 2θ values of 18.04°, 20.24°, and 36.19° in the XRD chart of PVdF-HFP membrane corresponding to (100), (020), and (021) crystal indices, respectively (Stephan et al., 2006)[see Fig. 5**a**]. Besides these defined PVdF-HFP membrane peaks, nickel species were identified through three characteristic planes at 42.77° (111), 49.75° (200), and 73.60° (220) to ascertain the formation of the face-centered cubic crystalline structure of nickel [JCPDS card No. 04–0850] (Barakat and Kim, 2009) [see Fig. 5**b**]. **The particle size of Ni nanoparticles is calculate used Scherrer equation** (Yao et al., 2016)**, it was found to be 19.5 nm.** It is worth mentioning that the reduced membrane in water media showed the same color as pristine PVDF-HFP spectra. As the membrane kept its green color. The stability of PVdF-HFP and Ni@PVdF-HFP membranes when subjected to elevated temperatures was examined through TGA charts in Fig. 6. One weight loss section was observed for bare HFP-10 film at 420 °C due to the random scission of its units during the degradation process

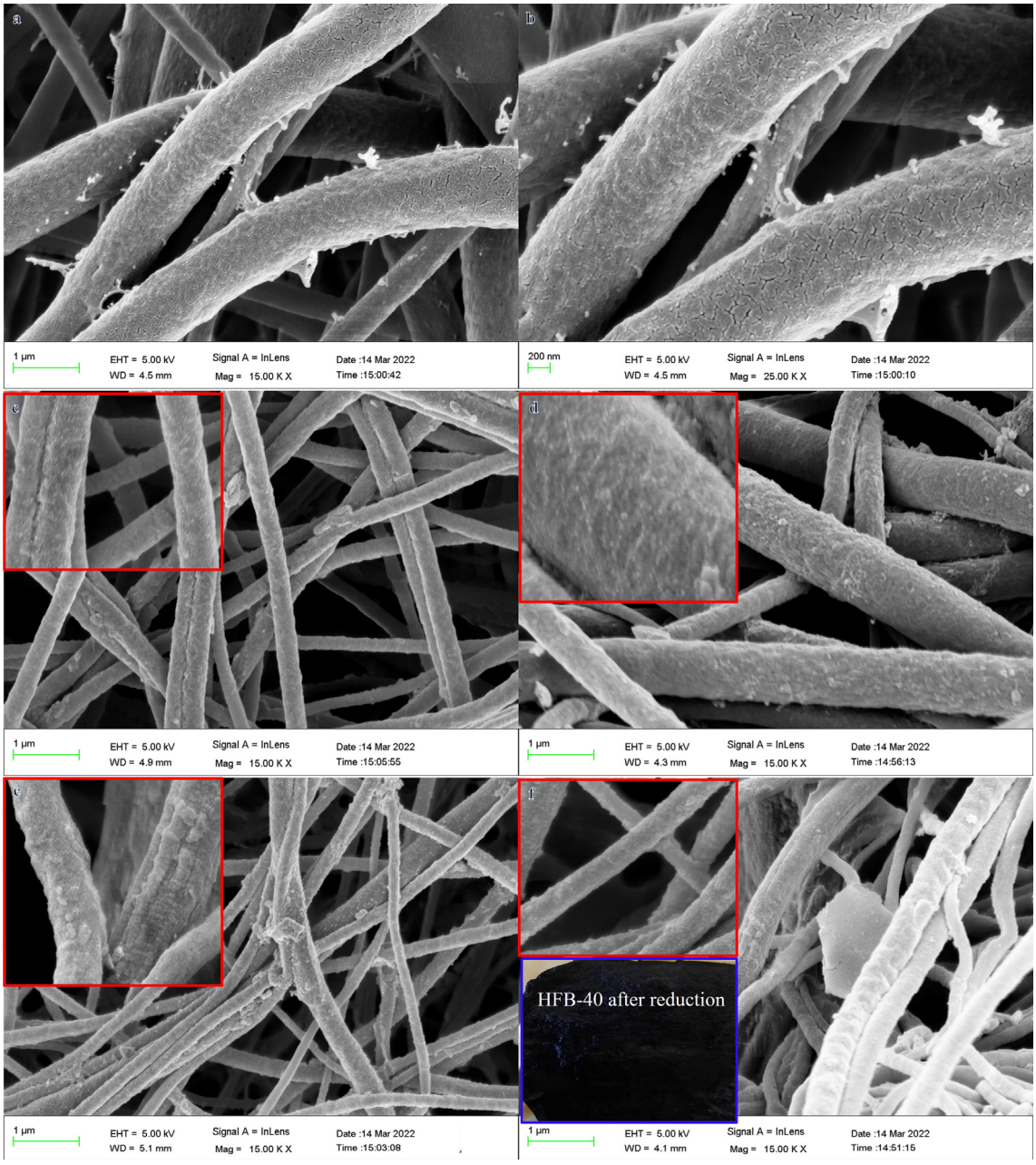

Fig. 2 SEM images of (A and B) PVdF-HFP, (C) HFB-10, (D) HFB-20, (E) HFB-30, and (C) HFB-40 membranes.

(Kim et al., 2011; Babu et al., 2015). This step was shown at a lower temperature value [346 °C] after nickel species were incorporated into HFP-10 film, besides a small change at 95 °C when physisorbed water molecules were evaporated. The presence of Ni NPs in the structure of this polymeric membrane was responsible for weakening the van der Waals′ interacting forces between its chains. This,facilitated the degradation of the metal-supporting polymeric membrane at decreased temperatures when related to the case at bare film (VijayaáKumar, 2001). FTIR spectra of PVdF-HFP and Ni@PVdF-HFP membranes were also described in Fig. 7. Common vibrational bands were noticed in both charts that depicted the polymeric membrane. Its α and β phases were confirmed by their respective peaks at frequency values of 749 and 837 cm^{-1} (Kumar and Nahm, 2008). Another two specific vibrational bands were centred at 672 and 872 cm^{-1} that were assigned for C – F and CH_2 wagging of vinylidene units in the amorphous phase of PVdF-HFP film. Furthermore, the symmetric C – F stretching, CF_2 stretching, and deformed vibrations in this membrane were also shown through their corresponding bands at 1071, 1175, and 1400 cm^{-1} (Mandal et al., 2014). Additional two peaks appeared when nickel precursor salt was introduced during the polymeric film fabrication. The formation of Ni – O species into this nanomaterial was supporting by its stretching vibration peaks at 1561 cm^{-1} (Nath, 2014).

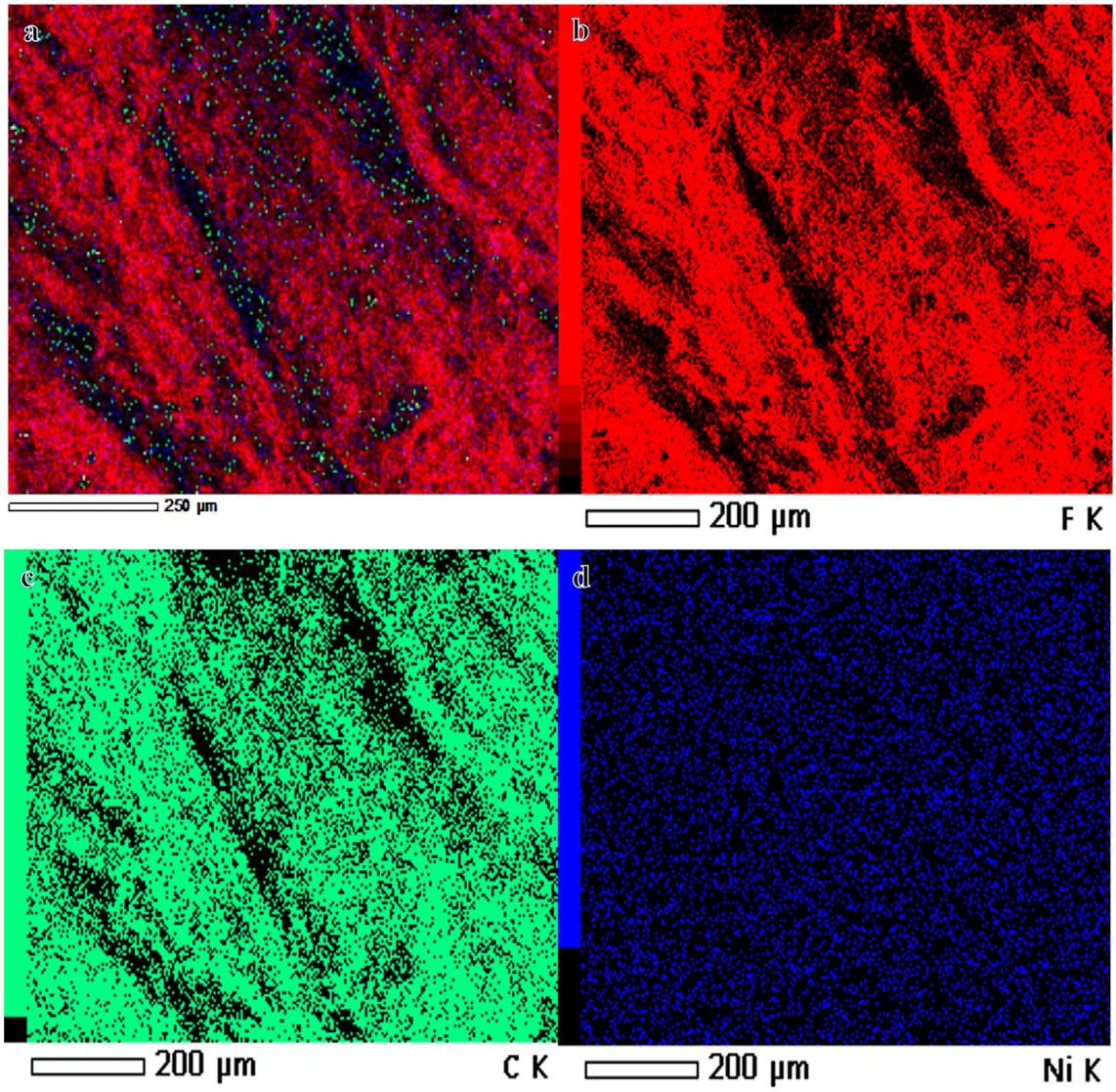

Fig. 3 Elemental mapping showing the distribution of fluorine (F), carbon (C) and nickel (Ni) in the HFB-40 membrane.

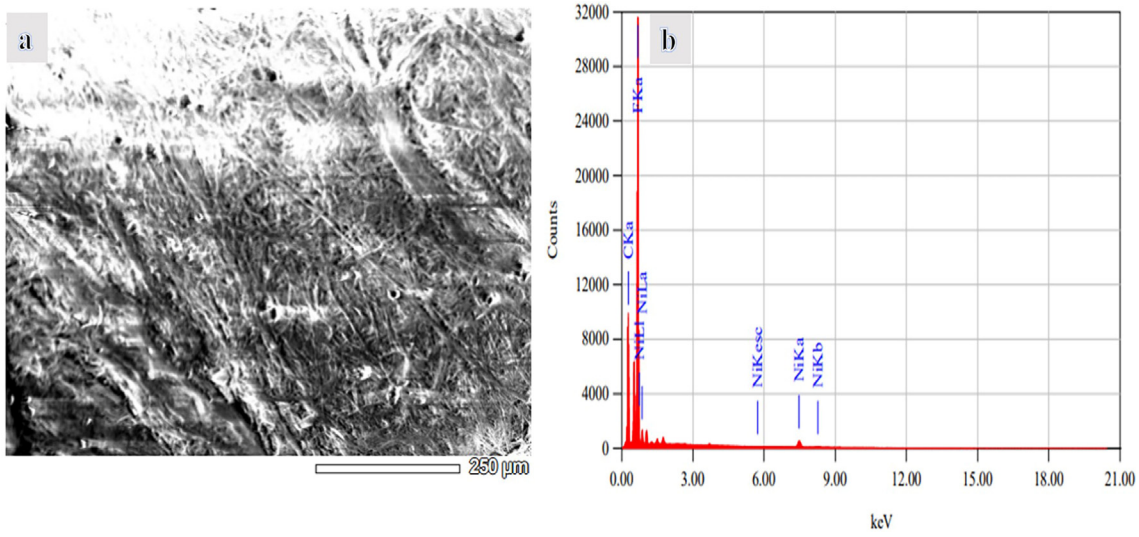

Fig. 4 (A) SEM image and (B) EDX chart of HFB-40 membrane.

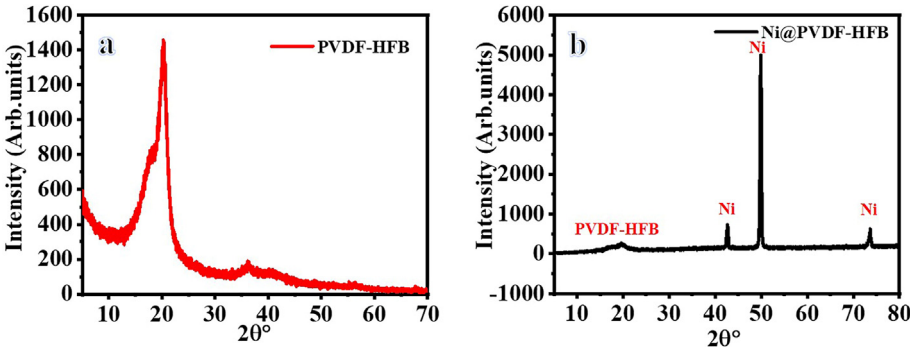

Fig. 5 XRD results of PVdF-HFP and HFP-40 membranes (A, B), respectively.

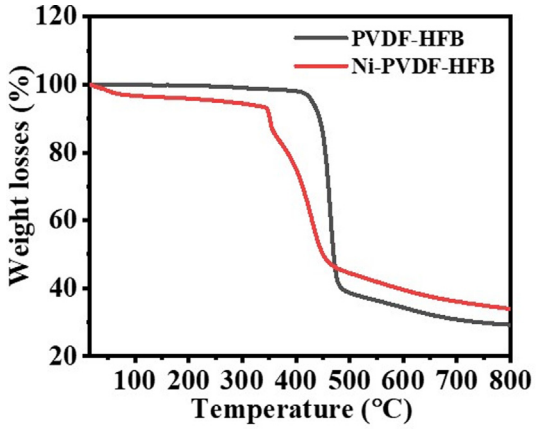

Fig. 6 TGA chart of PVdF-HFP and HFB-40 membranes.

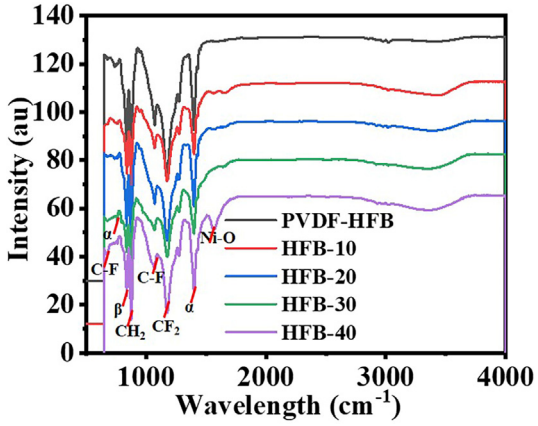

Fig. 7 FTIR charts of PVdF-HFP and Ni@PVdF-HFP membranes.

3.1. H_2 generation from sodium borohydride

Their shape influenced the catalytic activity of the catalysts. Shape-anisotropic nanostructures possessing more active sites for catalysis led to improved catalytic performance. NFs have a large surface area compared to other nanostructures, leading to better performance as catalyst support. Nonetheless, it was demonstrated that the nanofibrous morphologies corresponding to the long axial ratio provide a significant performance when compared to other nanostructures. In this regard, NFM outperforms typical powder-like catalysts in terms of catalyst separation and capacity to be reused. Ni@PVDF-HFP MNFs were prepared by electrospinning technique, tested as a catalyst in the hydrolysis of NABH4 and found to be the highly active catalyst to generate H_2. The hydrolysis of 1.34 mmol of alkaline $NaBH_4$ occurred without any catalyst; however, it obtained 28 mL after 60 min. The addition of pristine PVDF-HFP MNFs to 1.34 mmol of alkaline $NaBH_4$ did not significantly affect the $NaBH_4$ hydrolysis. However, **the H_2 generation is increased with a reduction in the time using electrospun Ni@PVdF-HFP MNFs** (Fig. 8), as shown by the variation in the catalytic activity using different Ni contents. Experiments were performed by adding 100 mg of MNFs from all formulations, in the separated glass reactor, into 1.34 mmol of alkaline $NaBH_4$ at 25 °C to determine the best activity of the synthesized membrane NFs. As manifested in the figure the HFP-40 (103 mL in 60 min) membrane, NFs have shown the highest H_2 generation rate than other ratios [HFB-10 (68 mL in 60 min), HFB-20 (81 mL in 60 min), and HFB-30 (93 mL in 60 min), so it has chosen to be used in further experiments. **The fabricated MNFs have shown better catalytic activity, and it produced 103 mL in 60 min using 1.34 mmol $NaBH_4$ and 100 mg catalyst at 25 °C, than PVDF-[C6(mpy)2][NiCl4]2 NFs composite catalyst** (Sheikh et al., 2011), **]; it was produced about 140 mL H_2 in 60 min used 158.72 mM $NaBH_4$ and 40 mg from the catalyst contain 2.5 % Ni, and 40 % Ni@TiO_2** (Dönmez and Ayas NJIJoHE. , 2021)**, it was produced 37.89 mL $H_2.g_{cat}^{-1}$ min^{-1} used 100 mg $NaBH_4$, 100 mg catalyst, 5 mL 0.25 M NaOH at 20 °C. Jaeyeong et al.** (Lee et al., 2019)**, demonstrated that the Ni powder needed the longest time (280 min) to generate the same amount of hydrogen (500 mL) compared with Ni thin film (240 min), and etched Ni foil (60 min) used 1.5 g $NaBH_4$ and 0.01 g from catalysts at 25 °C although Ni powder high surface area. This could be due to the easily contaminated or oxidized.** Accordingly, the rougher surface, which was made by in situ difficult reduction reaction of NiAc to metallic Ni on the surface of PVDF-HFP, made the catalyst more efficient. Catalytic hydrolysis of $NaBH_4$ depends on the type of catalyst and other parameters such as $NaBH_4$ concentration, reaction temperature, catalyst amount, and reusability. For this reason, the effect of these parameters on the hydrolysis of $NaBH_4$ was investigated in the presence of the HFB-40. The effect of $NaBH_4$ concentration on the reaction rate has been tested

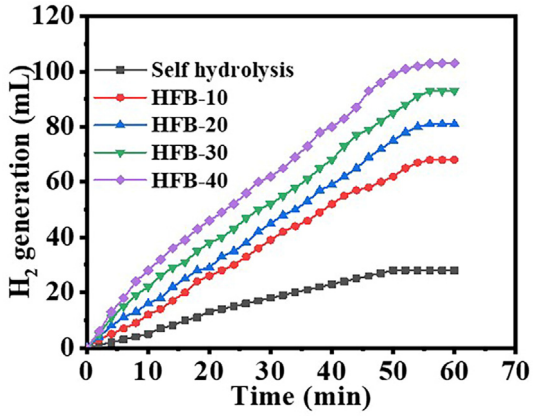

Fig. 8 The effect of Ni content of the Ni@PVdF-HFP membranes on H_2 generation from NABH4 hydrolysis.

(Fig. 9**a**) using 100 mg of HFP-40 MNFs at 25 °C. As shown in the figure, the initial H_2 generation rate is linearly increased with an increase in $NaBH_4$ concentration. When the amount of $NaBH_4$is increases from **50 mg to 125 mg**, the hydrogen production rate increases from **255.2 mL.g$^{-1}_{cat}$ min^{-1} to 689.9 mL.g$^{-1}_{cat}$ min^{-1}**, respectively. The estimated slope of the best-fit line was 0.74 (Fig. 9**b**), which clarifies that the H_2 production rate follows pseudo-first-order kinetics concerning $NaBH_4$. This is due to the use of low $NaBH_4$ concentration as the higher concentration follows the pseudo-zero order reaction, in which at higher concentration, the viscosity increases, the reactant diffusion resistance, reaction rate decreases, and the by-product ($NaBO_2$) formed in hydrolysis can adsorb on the catalyst surface and block the active sites (Ozay et al., 2011; Sagbas, 2012; Walter et al., 2008; Saka and Eygi, 2020). Our study was investigated at low concentration compared to the zero-order reaction. To examine the influence of the reaction temperature effect (Fig. 10), experiments were executed using 2.67 mmol of alkaline $NaBH_4$with 100 mg of HFP-40 MNFs at temperatures ranging from 298 K to 328 K to obtain the activation energy (E_a) of $NaBH_4$hydrolysis catalyzed HFB-40 using the Arrhenius equation (**Eq. (4)**).

$$lnk = lnA - \frac{E_a}{RT} \tag{4}$$

Where k is a rate constant, A is a pre-exponential factor, R is a gas constant, and T is the reaction temperature. As expected, the H_2 generation increased as the reaction temperature and H2 volume vs reaction time changed linearly (Fig. 10a). As shown in the figure, the reaction time for H2 generation has been reduced at elevated temperature. Furthermore, **the H_2 generation is increased**. As seen in Fig. 10, when the reaction temperature rises from 25 °C to 55 °C, the hydrogen yield increases from 50 % to 100 % in 28 min. This obtained is compatible with the studies in the literature (Ekinci et al., 2020; Wei et al., 2017; Li et al., 2014). The rate (k) value is obtained from the linear portion of temperature graphs. From Arrhenius plot ln (k) versus 1/T in Fig. 10**b** and Arrhenius equation (**Eq. (2)**), the E_a was estimated to be 23.52 kJ mol^{-1}. Activation energies of non-noble metals were reported in the literature between 16.28 and 42.45 kJ mol-1 (Dönmez and Ayas NJIJoHE. , 2021; Tamboli et al., 2015; Hua et al., 2003; Soltani, 2020; Kılınç and Şahin, 2019). Activation energy values of prepared NFs and Ni-based catalysts are compared (Table1), indicating superior catalytic performance of the introduced Ni@PVDF-HFP. The H_2 generation gathered over time by employing different catalyst amounts (100 to 250 mg) of HFP-40 MNFs is given in Fig. 11. As expected, **the H_2 generation increased when the amount of HFP-40 was increased as more catalyst provides** more active sites for $NaBH_4$ dehydrogenation. One can note that the H_2 generation from the hydrolysis reaction of $NaBH_4$ proceeds very slowly and then stops without catalyst (Fig. 8). The H_2 generation increased as the catalyst amount increased (Fig. 11**a**), attributed to the fact that hydrolysis reaction of $NaBH_4$ is a catalyst-controlled reaction. This phenomenon can be attributed to the fact that the reaction rate increased due to the active sites of the catalyst increasing in direct proportion to catalyst amount, called structure sensitivity. Thus, it is clear that H_2 generation can be determined by controlling catalyst amount. Fig. 11**b** shows the ln H_2 generation rate vs ln HFB-40. The determined slope of the best-fit line is 1.29, suggesting that the produced H_2 agrees with pseudo-first-order kinetics regarding the amount of catalyst. According to the results obtained from the effect of catalyst concentration, $NaBH_4$ concentration, and reaction temperature, the $NaBH_4$ dehydrogenation kinetic equation catalyzed by the introduced NFs membrane can be written according to Eqs. (5), (6), and (7).

$$r = -d[SBH]dt = k[HFB - 40]^{1.29}[SBH]^{0.74} \tag{5}$$

$$k = Ae^{\left(\frac{-E_a}{RT}\right)} \rightarrow \ln k = \ln A - \frac{E_a}{RT} \tag{6}$$

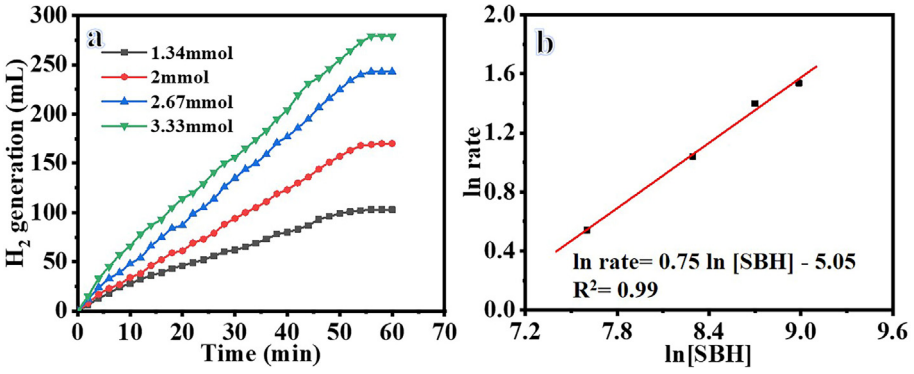

Fig. 9 The effect of NAaBH$_4$ concentration on H_2 generation from $NaBH_4$ hydrolysis.

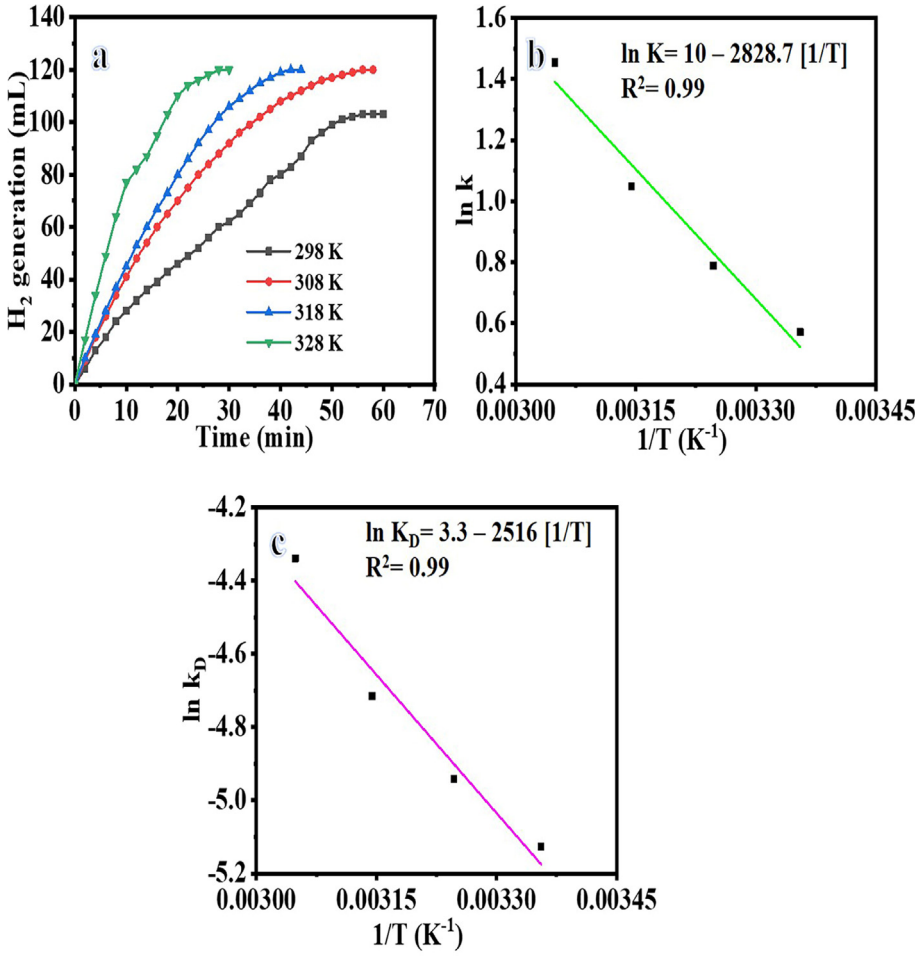

Fig. 10 The effect of reaction temperature on H_2 generation from $NaBH_4$ hydrolysis (a), logarithmic value of hydrogen generation rate constant vs (1/T) (b), and logarithmic value of the k_D (k/T) vs reciprocal of reaction temperature (c).

$$r = -d[SBH]dt$$
$$= 22337.01e^{\left(\frac{2828.7}{T}\right)}[HBF - 40]^{1.29}[SBH]0.74 \quad (7)$$

Gibbs free energy of activation (ΔG, (kJ mol^{-1})) can be determined using thermodynamic data (activation enthalpy (ΔH, (kJ mol^{-1})) and activation entropy (ΔS, (J mol^{-1} K^{-1})) according to Eqs. (8) and (9):

$$\ln k_D = \ln\frac{k_B}{h} + \frac{\Delta S}{R} - \frac{\Delta H}{RT} \quad (8)$$

$$\Delta G = \Delta H - T\Delta S \quad (9)$$

Where k_D = (k/T), K_B and h are the Boltzmann constant (1.381×10^{-23} J K^{-1}) and the Planck constant (6.626×10^{-34} J s^{-1}), respectively. According to Eq. (9) and Fig. 10, ΔH and ΔS is estimated to be 20.92 kJ mol^{-1} and 0.0272 kJ mol^{-1}, respectively. ΔG equation can be summarized as follows:

$$\Delta G = 20.92 - 0.0272T \quad (10)$$

ΔG values are estimated to be 12.81 and 11.9 kJ mol^{-1} at 298 and 323 K, respectively. This main that the reaction's spontaneity is directly increased with the temperature.

Reusability and stability are significant factors in determining whether the catalyst is suitable for a practical application. The reusability of the HFB-40 membrane NFs was tested repeatedly ten times to confirm its stability in the presence of 2.67 mmol of alkaline $NaBH_4$, at each cycle, with 100 mg of HFP-40 MNFs at 25 °C (Fig. 12). The membrane NFs was used ten times without makeup, reactivation, or regeneration. As seen in the figure, the catalytic activity of the membrane NFs catalyst is maintained even if the use is repeated for up to 8 cycles as the H_2 generation rate remains unchanged. The slight decreases have been demonstrated as the cycle number increases. The same amount of H2 has been generated extended reaction time. This could be due to the precipitate of reaction products on the membrane that inhibited the active metal sites as the membrane is used without cleaning during all cycles, which this accumulation harms the hydrogen generation rate. The slight decrease in catalytic activity after eight cycles may be due to the increase in the number of boron products on the membrane surface as an increase in the solution viscosity (Yang et al., 2017), which decreases the accessibility of active sites or blockage of pores in the membrane NFs. XPS of the HFB-40 catalyst confirms this after reuse for ten cycles (Fig. 13). The Ni 2p XPS spectrum of Ni 2p spectra shows two main peaks positioned at 856.1 and 873.6 eV, which are assigned to Ni 2P3/2 and Ni 2P1/2, together with two corresponding satellite peaks located at 861.7 and 880.6 eV (Zhu et al., 2017). As depicted in Figure, the Ni 2p3 peak located at 856.1 eV demonstrated the formation of $Ni(OH)_2$ after reuse

Table 1 The activation energies of membrane NFs and nickel-based catalysts in H_2 production using sodium borohydride.

Catalyst	E_a (KJ/mol)	Ref.
Ni	42.28	(Ozay et al., 2011)
Ni	71	(Kaufman, 1985)
Raney Ni	63	(Kaufman, 1985)
Co-Ni/AC	68.9	(Didehban and Zabihi, 2018)
Hydrogen phosphate-stabilized Ni(0) nanoclusters	54	(Kılınç and Şahin ÖJIJoHE. , 2019)
Ni(0)	51.4	(Yang et al., 2017)
Ni/TiO_2	25.11	(Chaugule et al., 2015)
Ni-hollow PVDF capsules	49.3	(Chen et al., 2015)
Ni-PVDF hollow fiber	55.3	(Chen et al., 2015)
$([C6(mpy)2][NiCl4]^{2-}$	56.4	(Chinnappan et al., 2012)
PVDF-$[C6(mpy)2][NiCl4]^{2-}$	44.6	(Chinnappan and Kim HJIjohe. Nanocatalyst, , 2012)
Co-Ni/MWAC	40.7	(Soltani, 2020)
Sm- Ni-Co-P/g-Al_2O_3	52.1	(Li et al., 2014)
Ni–Co–B	62	(Ingersoll et al., 2007)
HFB-40	23.5	This study

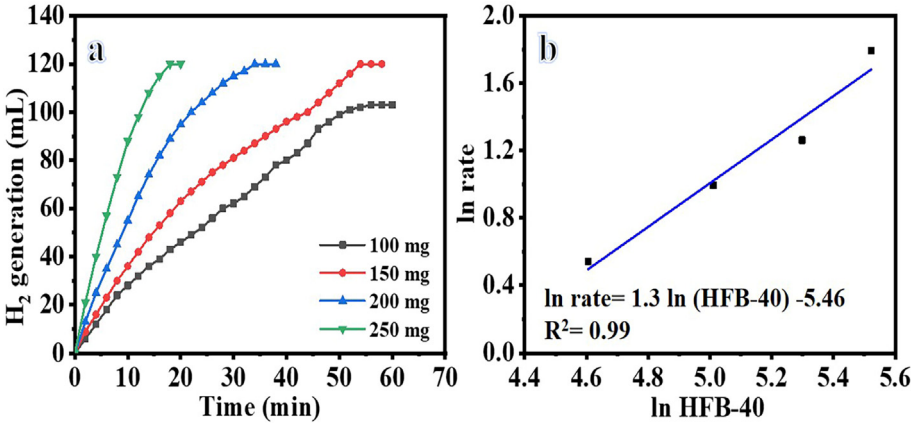

Fig. 11 The effect of HFB-40 membrane amount on H_2 generation from $NaBH_4$ hydrolysis.

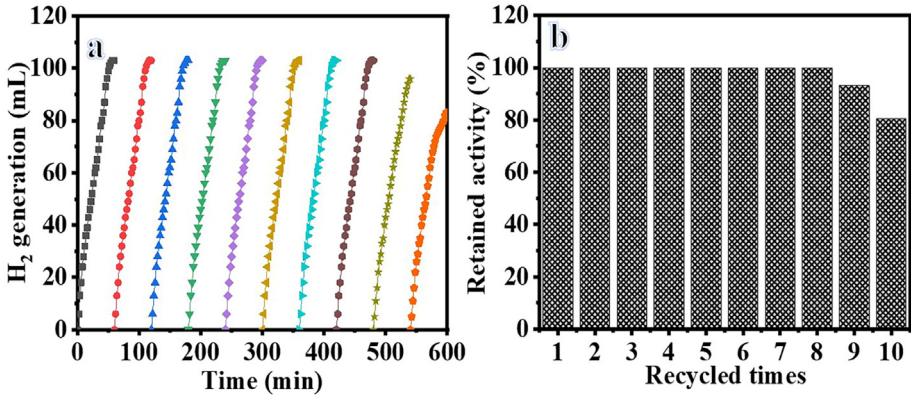

Fig. 12 Reusability test of HFB-40.

ten times, which is similar to the value obtained in literature (Yao et al., 2016). Furthermore, Na 1 s peak located at 1072.2 eV and B 1 s peak located at 180 eV appeared after reuse, ten cycles because the Na ions are generated from $NaBH_4$ hydrolysis, which mainly constitutes contaminants, are dissolved in the solution during the hydrolysis. The SEM image of HFB-40 catalyst after reuse for ten cycles (Fig. 14) indicates that the NFS kept their nanofibrous structure.

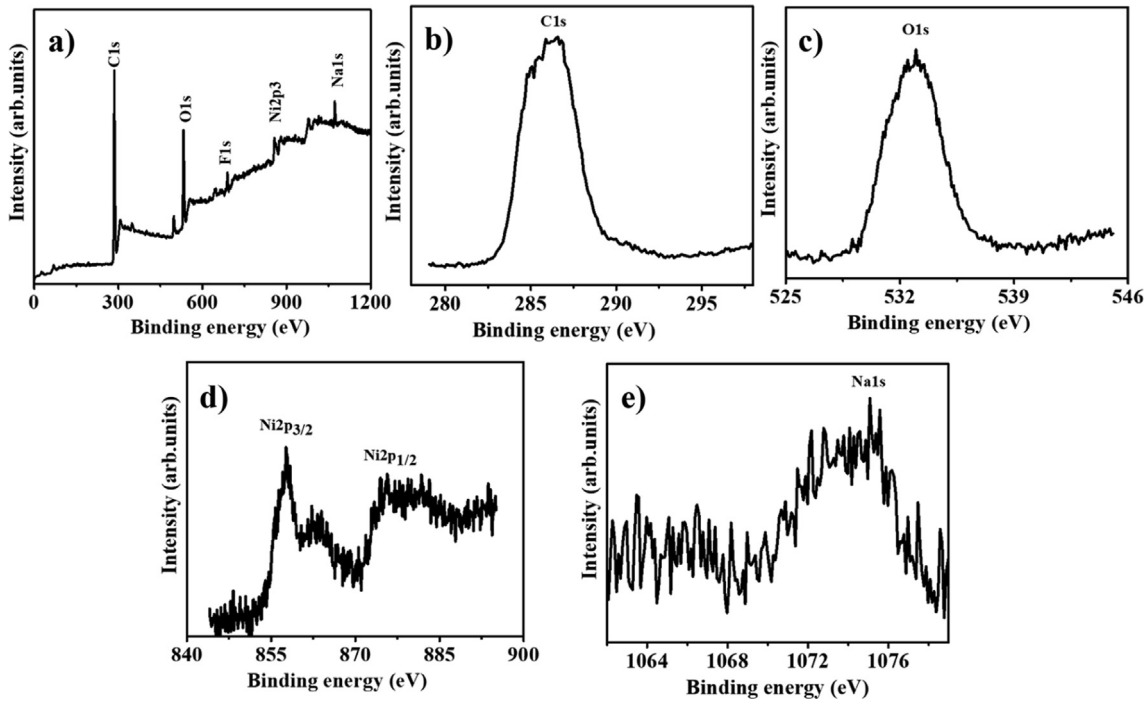

Fig. 13 a) survey spectrum of HFB-40, b) C1s, c) O1s, d) Ni2p and e) Na1s XPS spectra of HFB-40 membrane after ten cycles reused.

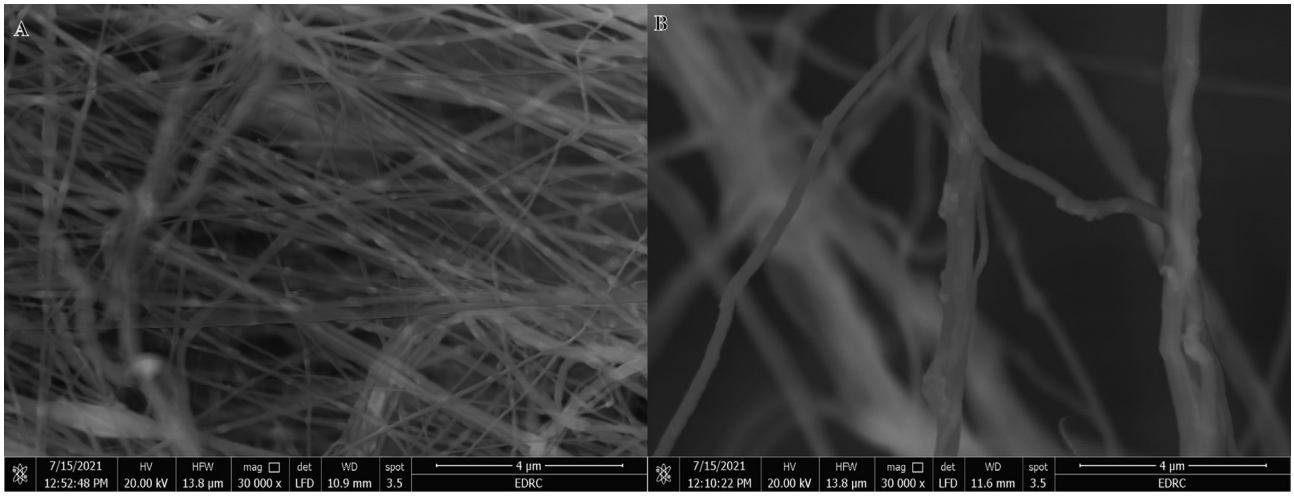

Fig. 14 Low (a) and high magnifications (b) of HFB-40 membrane after ten cycles reused.

4. Conclusion

Metallic Ni NPs @ PVDF-HFP membrane NFs catalysts have been successfully prepared via electrospinning technique followed by in-situ reduction of metal ions to metallic Ni. The prepared metal catalysts have shown an excellent catalytic performance in the H_2 generation from $NaBH_4$. The sample was composed of 40 %wt. NiAc showed the highest catalytic activity compared to the other formulations. Whereas 103 mL of H_2, from the hydrolysis of 1.34 mmol $NaBH_4$, was produced using 40 % wt. NiAc tis compared to 68 mL, 81 mL, and 93 mL for 10 % wt., 20 % wt., and 30 % wt. NiAc, respectively, in 60 min at 25 °C. The increase in the temperature lead to an increase in the hydrogen production rate and obtained low activation energy. (23.52 kJ mol^{-1}). The kinetics study revealed that the reaction was pseudo-first-order in sodium borohydride concentration and catalyst amount.

Furthermore, the catalyst exhibits satisfactory stability in the hydrolysis process for ten cycles. Because of its easy recyclability, the introduced catalyst has a wide range of potential applications in the generation of H_2 from sodium borohydride hydrolysis. Considering that the eco-friendly and inexpensive Ni@PVDF-HFP membrane NFs are catalytically effective with superior reusability, they should have potential application in the H_2 generation from the sodium borohydride hydrolysis.

CRediT authorship contribution statement

Abdullah M. Al-Enizi: Conceptualization, Investigation, Methodology, Writing – original draft. **Ayman Yousef:** Conceptualization, Data curation, Investigation, Methodology, Writing – original draft, Writing – review & editing. **Shoyebmohamad F. Shaikh:** Conceptualization, Investigation, Methodology, Writing – review & editing. **Bidhan Pandit:** Methodology, Writing – review & editing. **M.M. El-Halwany:** Investigation, Methodology, Validation.

Declaration of Competing Interest

The authors declare that they have no known competing financial interests or personal relationships that could have appeared to influence the work reported in this paper.

Acknowledgement

The authors extend their sincere appreciation to the Researchers Supporting Project number (RSP-2021/370), King Saud University, Riyadh, Saudi Arabia, for the financial support.

Appendix A. Supplementary material

Supplementary data to this article can be found online at https://doi.org/10.1016/j.arabjc.2022.104207.

References

Abdelhamid, H.N., 2021. A review on hydrogen generation from the hydrolysis of sodium borohydride. Int. J. Hydrogen Energy 46, 726–765.

Abdelhamid, H.N., 2021. Solid acid zirconium oxo sulfate/carbon-derived UiO-66 for hydrogen production. Energy Fuels 35, 10322–10326.

Arzac G, Rojas TC, Fernández AJACBE. New insights into the synergistic effect in bimetallic-boron catalysts for hydrogen generation: the Co–Ru–B system as a case study. 2012;128:39-47.

Aydın K, Kulaklı BN, Coşkuner Filiz B, Alligier D, Demirci UB, Kantürk Figen AJIJoER. Closing the hydrogen cycle with the couple sodium borohydride-methanol, via the formation of sodium tetramethoxyborate and sodium metaborate. 2020;44:11405-16.

Babu KJ, Yoo DJ, Kim ARJRA. Binder free and free-standing electrospun membrane architecture for sensitive and selective non-enzymatic glucose sensors. 2015;5:41457-67.

Barakat NA, Kim B, Kim HYJTJoPCC. Production of smooth and pure nickel metal nanofibers by the electrospinning technique: nanofibers possess splendid magnetic properties. 2009;113:531-6.

Cai H, Lu P, Dong JJF. Robust nickel–polymer nanocomposite particles for hydrogen generation from sodium borohydride. 2016;166:297-301.

Cai, H., Liu, L., Chen, Q., Lu, P., Dong, J., 2016. Ni-polymer nanogel hybrid particles: a new strategy for hydrogen production from the hydrolysis of dimethylamine-borane and sodium borohydride. J. Energy 99, 129–135.

Calabretta, D.L., Davis, B.R., 2007. Investigation of the anhydrous molten Na–B–O–H system and the concept: electrolytic hydriding of sodium boron oxide species. J. Power Sources 164, 782–791.

Chaugule AA, Tamboli AH, Sheikh FA, Kim HJC, Physicochemical SA, Aspects E. Preparation and application of Sm–Ni oxide doped TiO2 nanofiber as catalyst in hydrogen production from sodium borohydride hydrolysis. 2015;484:242-52.

Chen Y, Kim HJML. Ni/Ag/silica nanocomposite catalysts for hydrogen generation from hydrolysis of NaBH4 solution. 2008;62:1451-4.

Chen C-W, Chen C-Y, Huang Y-HJIjohe. Method of preparing Ru-immobilized polymer-supported catalyst for hydrogen generation from NaBH4 solution. 2009;34:2164-73.

Chen Y, Liu L, Wang Y, Kim HJFpt. Preparation of porous PVDF-NiB capsules as catalytic adsorbents for hydrogen generation from sodium borohydride. 2011;92:1368-73.

Chen Y, Shi Y, Wang YJIJoER. Preparation of hollow poly (vinylidene fluoride) capsules containing nickel catalyst for hydrogen storage and production. 2015;39:634-42.

Chen Y, Shi Y, Liu X, Zhang YJF. Preparation of polyvinylidene fluoride–nickel hollow fiber catalytic membranes for hydrogen generation from sodium borohydride. 2015;140:685-92.

Chinnappan A, Kim HJIjohe. Nanocatalyst: Electrospun nanofibers of PVDF–Dicationic tetrachloronickelate (II) anion and their effect on hydrogen generation from the hydrolysis of sodium borohydride. 2012;37:18851-9.

Chinnappan A, Kim H, Baskar C, Hwang ITJIjohe. Hydrogen generation from the hydrolysis of sodium borohydride with new pyridinium dicationic salts containing transition metal complexes. 2012;37:10240-8.

Chinnappan, A., Kang, H.-C., Kim, H., 2011. Preparation of PVDF nanofiber composites for hydrogen generation from sodium borohydride. J. Energy 36, 755–759.

Crisafulli C, Scirè S, Salanitri M, Zito R, Calamia SJIjohe. Hydrogen production through NaBH4 hydrolysis over supported Ru catalysts: an insight on the effect of the support and the ruthenium precursor. 2011;36:3817-26.

Didehban A, Zabihi M, Shahrouzi JRJIJoHE. Experimental studies on the catalytic behavior of alloy and core-shell supported Co-Ni bimetallic nano-catalysts for hydrogen generation by hydrolysis of sodium borohydride. 2018;43:20645-60

Dinc M, Metin Ö, Özkar SJCt. Water soluble polymer stabilized iron (0) nanoclusters: A cost-effective and magnetically recoverable catalyst in hydrogen generation from the hydrolysis of sodium borohydride and ammonia borane. 2012;183:10-6.

Ding X-L, Yuan X, Jia C, Ma Z-FJijohe. Hydrogen generation from catalytic hydrolysis of sodium borohydride solution using cobalt–copper–boride (Co–Cu–B) catalysts. 2010;35:11077-84.

Dönmez F, Ayas NJIJoHE. Synthesis of Ni/TiO2 catalyst by sol-gel method for hydrogen production from sodium borohydride. 2021;46:29314-22.

Ekinci A, Cengiz E, Kuncan M, Şahin ÖJIJoHE. Hydrolysis of sodium borohydride solutions both in the presence of Ni–B catalyst and in the case of microwave application. 2020;45:34749-60.

Gibson P, Schreuder-Gibson H, Rivin DJC, Physicochemical SA, Aspects E. Transport properties of porous membranes based on electrospun nanofibers. 2001;187:469-81

Hua D, Hanxi Y, Xinping A, Chuansin CJIJoHE. Hydrogen production from catalytic hydrolysis of sodium borohydride solution using nickel boride catalyst. 2003;28:1095-100

Ingersoll J, Mani N, Thenmozhiyal J, Muthaiah AJJoPS. Catalytic hydrolysis of sodium borohydride by a novel nickel–cobalt–boride catalyst. 2007;173:450-7.

Kang H-C, Chen Y, Arthur EE, Kim HJIjohe. Microstructural control of catalyst-loaded PVDF microcapsule membrane for hydrogen generation by NaBH4 hydrolysis. 2014;39:15656-64.

Kassem, A.A., Abdelhamid, H.N., Fouad, D.M., Ibrahim, S.A., 2019. Metal-organic frameworks (MOFs) and MOFs-derived CuO@ C for hydrogen generation from sodium borohydride. Int. J. Hydrogen Energy 44, 31230–31238.

Kaufman CM, Sen BJJotCS, Dalton Transactions. Hydrogen generation by hydrolysis of sodium tetrahydroborate: effects of acids and transition metals and their salts. 1985:307-13.

Kılınç D, Şahin, Ömer Synthesis of polymer supported Ni (II)-Schiff Base complex and its usage as a catalyst in sodium borohydride

hydrolysis. International Journal of Hydrogen Energy. 2018;43:10717-27

Kılınç D, Şahin ÖJIJoHE. Effective TiO2 supported Cu-Complex catalyst in NaBH4 hydrolysis reaction to hydrogen generation. 2019;44:18858-65.

Kim AR, Nahm KS, Yoo DJJCAP. High proton conductivity and low fuel crossover of polyvinylidene fluoride–hexafluoro propylene–silica sulfuric acid composite membranes for direct methanol fuel cells. 2011;11:896-902

Kim J-H, Lee, Ho, Han, Sang-Cheol, Kim, Hyun-Seok, Song, Min-Sang, Lee, Jai-Young Production of hydrogen from sodium borohydride in alkaline solution: development of catalyst with high performance. International Journal of Hydrogen Energy. 2004;29:263-7.

Kumar GGJJoMC. Irradiated PVdF-HFP-montmorillonite composite membranes for the application of direct ethanol fuel cells. 2011;21:17382-91.

Kumar GG, Nahm KS, Elizabeth RNJJoMS. Electro chemical properties of porous PVdF-HFP membranes prepared with different nonsolvents. 2008;325:117-24

Larichev YV, Netskina O, Komova O, Simagina VJIJoHE. Comparative XPS study of Rh/Al2O3 and Rh/TiO2 as catalysts for NaBH4 hydrolysis. 2010;35:6501-7.

Lee J, Shin H, Choi KS, Lee J, Choi J-Y, Yu HKJIJoHE. Carbon layer supported nickel catalyst for sodium borohydride (NaBH4) dehydrogenation. 2019;44:2943-50.

Lee Y-J, Badakhsh, Arash, Min, Dongsu, Jo, Young Suk, Sohn, Hyuntae, Yoon, Chang Won, Jeong, Hyangsoo, Kim, Yongmin, Kim, Kwang-Bum, Nam, Suk Woo. Development of 3D open-cell structured Co-Ni catalysts by pulsed electrodeposition for hydrolysis of sodium borohydride. Applied Surface Science. 2021;554:149530.

Lee Y-J, Badakhsh A, Min D, Jo YS, Sohn H, Yoon CW, et al. development of 3D open-cell structured Co-Ni catalysts by pulsed electrodeposition for hydrolysis of sodium borohydride. 2021;554:149530.

Li F, Arthur EE, La D, Li Q, Kim HJE. Immobilization of CoCl2 (cobalt chloride) on PAN (polyacrylonitrile) composite nanofiber mesh filled with carbon nanotubes for hydrogen production from hydrolysis of NaBH4 (sodium borohydride). 2014;71:32-9

Li Q, Chen Y, Lee DJ, Li F, Kim HJE. Preparation of Y-zeolite/CoCl2 doped PVDF composite nanofiber and its application in hydrogen production. 2012;38:144-50

Li Z, Li H, Wang L, Liu T, Zhang T, Wang G, et al. Hydrogen generation from catalytic hydrolysis of sodium borohydride solution using supported amorphous alloy catalysts (Ni–Co–P/γ-Al2O3). 2014;39:14935-41.

Liu W, Cai H, Lu P, Xu Q, Zhongfu Y, Dong JJIjohe. Polymer hydrogel supported Pd–Ni–B nanoclusters as robust catalysts for hydrogen production from hydrolysis of sodium borohydride. 2013;38:9206-16.

Lo C-tF, Karan K, Davis BRJI, research ec. Kinetic studies of reaction between sodium borohydride and methanol, water, and their mixtures. 2007;46:5478-84.

Mališ J, Mazúr P, Schauer J, Paidar M, Bouzek KJIjohe. Polymer-supported 1-butyl-3-methylimidazolium trifluoromethanesulfonate and 1-ethylimidazolium trifluoromethanesulfonate as electrolytes for the high temperature PEM-type fuel cell. 2013;38:4697-704.

Mandal BP, Vasundhara K, Abdelhamid E, Lawes G, Salunke HG, Tyagi AKJTJoPCC. Improvement of magnetodielectric coupling by surface functionalization of nickel nanoparticles in Ni and polyvinylidene fluoride nanohybrids. 2014;118:20819-25

Nath A, Kumar AJJoms. Swift heavy ion irradiation induced enhancement in electrochemical properties of ionic liquid based PVdF-HFP-layered silicate nanocomposite electrolyte membranes. 2014;453:192-201.

Oh TH, Gang BG, Kim H, Kwon SJE. Sodium borohydride hydrogen generator using Co–P/Ni foam catalysts for 200 W proton exchange membrane fuel cell system. 2015;90:1163-70

Ozay O, Aktas N, Inger E, Sahiner NJIjohe. Hydrogel assisted nickel nanoparticle synthesis and their use in hydrogen production from sodium boron hydride. 2011;36:1998-2006

Özhava D, Kılıcaslan NZ, Özkar SJACBE. PVP-stabilized nickel (0) nanoparticles as catalyst in hydrogen generation from the methanolysis of hydrazine borane or ammonia borane. 2015;162:573-82

Park J-H, Shakkthivel P, Kim H-J, Han M-K, Jang J-H, Kim Y-R, et al. investigation of metal alloy catalyst for hydrogen release from sodium borohydride for polymer electrolyte membrane fuel cell application. 2008;33:1845-52

Raghavan P, Zhao X, Kim J-K, Manuel J, Chauhan GS, Ahn J-H, et al. Ionic conductivity and electrochemical properties of nanocomposite polymer electrolytes based on electrospun poly (vinylidene fluoride-co-hexafluoropropylene) with nano-sized ceramic fillers. 2008;54:228-34

Ritter JA, Ebner, Armin D, Wang, Jun, Zidan, Ragaiy Implementing a hydrogen economy. J Materials Today. 2003;6:18-23.

Sagbas S, Sahiner NJFpt. A novel p (AAm-co-VPA) hydrogel for the Co and Ni nanoparticle preparation and their use in hydrogel generation from NaBH4. 2012;104:31-6.

Saka C, Eygi MS, Balbay AJIJoHE. CoB doped acid modified zeolite catalyst for enhanced hydrogen release from sodium borohydride hydrolysis. 2020;45:15086-99

Santos, D., 2010. Sequeira, CAC On the electrosynthesis of sodium borohydride. Int. J. Hydrogen Energy 35, 9851–9861.

Santos, D., Sequeira, C.A.C., 2011. Sodium borohydride as a fuel for the future. J. Renew. Sustain. Energy Rev. 15, 3980–4001.

Seven F, Sahiner NJJoPS. Enhanced catalytic performance in hydrogen generation from NaBH4 hydrolysis by super porous cryogel supported Co and Ni catalysts. 2014;272:128-36.

Sheikh FA, Cantu T, Macossay J, Kim HJSoam. Fabrication of poly (vinylidene fluoride)(PVDF) nanofibers containing nickel nanoparticles as future energy server materials. 2011;3:216-22.

Shen X, Wang Q, Wu Q, Guo S, Zhang Z, Sun Z, et al. CoB supported on Ag-activated TiO2 as a highly active catalyst for hydrolysis of alkaline NaBH4 solution. 2015;90:464-74

Shin J, Nho Y-C, seon Hwang I, Fei G, Kim AR, Nahm KSJJoMS. Irradiated PVdF-HFP–tin oxide composite membranes for the applications of direct methanol fuel cells. 2010;350:92-100.

Soltani M, Zabihi MJIJoHE. Hydrogen generation by catalytic hydrolysis of sodium borohydride using the nano-bimetallic catalysts supported on the core-shell magnetic nanocomposite of activated carbon. 2020;45:12331-46.

Stephan AM, Nahm KS, Kulandainathan MA, Ravi G, Wilson JJEPJ. Poly (vinylidene fluoride-hexafluoropropylene)(PVdF-HFP) based composite electrolytes for lithium batteries. 2006;42:1728-34

Tamboli AH, Chaugule AA, Sheikh FA, Chung W-J, Kim HJE. Synthesis and application of CeO2–NiO loaded TiO2 nanofiber as novel catalyst for hydrogen production from sodium borohydride hydrolysis. 2015;89:568-75

Tian, X., Jiang, X., 2008. Poly(vinylidene fluoride-co-hexafluoropropene) (PVDF-HFP) membranes for ethyl acetate removal from water. J. Hazard. Mater. 153, 128–135.

VijayaáKumar RJJoMC. Sonochemical synthesis of amorphous Cu and nanocrystalline Cu2O embedded in a polyaniline matrix. 2001;11:1209-13.

Vijayakumar, E., Subramania, A., Fei, Z., Dyson, P.J., 2015. High-performance dye-sensitized solar cell based on an electrospun poly (vinylidene fluoride-co-hexafluoropropylene)/cobalt sulfide nanocomposite membrane electrolyte. RSC Adv. 5, 52026–52032.

Walter JC, Zurawski A, Montgomery D, Thornburg M, Revankar SJJoPS. Sodium borohydride hydrolysis kinetics comparison for nickel, cobalt, and ruthenium boride catalysts. 2008;179:335-9

Wang J, Yang L-j, Zhao X-c, Yang P, Cao W, Huang Q-sJIJoM, Metallurgy, et al. Highly efficient nanocatalyst Ni 1 Co 9@ graphene for hydrolytic dehydrogenation of sodium borohydride. 2021;27:1-7.

Wechsler D, Cui Y, Dean D, Davis B, Jessop PGJJotACS. Production of H2 from combined endothermic and exothermic hydrogen carriers. 2008;130:17195-203.

Wei Y, Wang R, Meng L, Wang Y, Li G, Xin S, et al. Hydrogen generation from alkaline NaBH4 solution using a dandelion-like Co–Mo–B catalyst supported on carbon cloth. 2017;42:9945-51

Xu D, Dai P, Liu X, Cao C, Guo QJJoPS. Carbon-supported cobalt catalyst for hydrogen generation from alkaline sodium borohydride solution. 2008;182:616-20

Yan J-M, Zhang X-B, Han S, Shioyama H, Xu QJIc. Synthesis of longtime water/air-stable Ni nanoparticles and their high catalytic activity for hydrolysis of ammonia− borane for hydrogen generation. 2009;48:7389-93.

Yang K, Yao Q, Huang W, Chen X, Lu Z-HJijohe. Enhanced catalytic activity of NiM (M = Cr, Mo, W) nanoparticles for hydrogen evolution from ammonia borane and hydrazine borane. 2017;42:6840-50.

Yao, Q., Shi, Y., Zhang, X., Chen, X., Lu, Z.H., 2016. Facile synthesis of platinum–cerium (IV) oxide hybrids arched on reduced graphene oxide catalyst in reverse micelles with high activity and durability for hydrolysis of ammonia borane. Chem.– Asian J. 11, 3251–3257.

Yao, Q., Ding, Y., Lu, Z.-H., 2020. Noble-metal-free nanocatalysts for hydrogen generation from boron-and nitrogen-based hydrides. Inorg. Chem. Front. 7, 3837–3874.

Yousef A, Barakat NA, Al-Deyab SS, Nirmala R, Pant B, Kim HYJC, et al. Encapsulation of CdO/ZnO NPs in PU electrospun nanofibers as novel strategy for effective immobilization of the photocatalysts. 2012;401:8-16

Zhang Y, Zhao Y, Bakenov Z, Gosselink D, Chen PJJoSSE. Poly (vinylidene fluoride-co-hexafluoropropylene)/poly (methyl-methacrylate)/nanoclay composite gel polymer electrolyte for lithium/sulfur batteries. 2014;18:1111-6.

Zhang, P., Li, R., Huang, J., Liu, B., Zhou, M., Wen, B., et al, 2021. Flexible poly(vinylidene fluoride-co-hexafluoropropylene)-based gel polymer electrolyte for high-performance lithium-ion batteries. RSC Adv. 11, 11943–11951.

Zhang H, Xu, Guochang, Zhang, Lu, Wang, Wenfeng, Miao, Wenkang, Chen, Kangli, Cheng, Lina, Li, Yuan, Han, Shumin Ultrafine cobalt nanoparticles supported on carbon nanospheres for hydrolysis of sodium borohydride. J Renewable Energy. 2020;162:345-54.

Zhu, D., Guo, C., Liu, J., Wang, L., Du, Y., Qiao, S.-Z., 2017. Two-dimensional metal–organic frameworks with high oxidation states for efficient electrocatalytic urea oxidation. Chem. Commun. 53, 10906–10909.